https://doi.org/10.15407/ujpe70.9.609

S.I. SHULYMA,[1] I.V. SUKHENKO,[1] V.KH. KASYANENKO,[2] V.L. KARBIVSKYY,[1] N.A. KURGAN,[1] N.K. SHVACHKO,[1] V.V. ZAIKA,[1] V.O. MOSKALIUK,[1] O.A. PUZKO[1]

[1] G.V. Kurdyumov Institute for Metal Physics, Nat. Acad. of Sci. of Ukraine
(36, Acad. Vernadsky Str., Kyiv 03680, Ukraine; e-mail: ser.shulyma@gmail.com)
[2] Vinnytsia National Technical University
(95, Khmelnytske Shosse, Vinnytsia 21021, Ukraine)

POWER-DEPENDENT EVOLUTION OF STRUCTURE AND OPTICAL PROPERTIES IN GALLIUM-DOPED ZnO MAGNETRON SPUTTERING THIN FILMS: EXPERIMENTAL AND DFT + U EXPLORATION

The effect of radiofrequency magnetron sputtering power on the morphology and optical properties gallium-doped ZnO (GZO) thin films has been investigated. It is found that the sputtering power increasing leads to a decreasing in the size of clusters on the film surface and the thickness of the crystallite columnar structure. It is shown that the optical bandgap decreasing may be due to the appearance of interstitial defects in the crystal lattice. Despite maintaining, a constant weight ratio of ZnO and Ga in the initial target mixture, an Ga concentration increasing in GZO thin films is observed for higher sputtering powers. The formation mechanism for GZO thin films under increasing magnetron sputtering power is proposed. It is associated with the appearance of Zn and O interstitial inclusions in the ZnO crystal lattice. Density functional theory (DFT) calculations (with Hubbard correction, DFT + U) show that the increased Ga concentration does not cause a narrowing of the optical band gap. Instead, an increase in the Ga content leads to the appearance of additional electronic states in the valence band (– 5.0 eV), which is associated with Zn 3d and O 2p hybridization with Ga 4s and Ga 4p states, a Zn 3d and O 2p energy levels position changing due to changes in interatomic distances and bond symmetry, and a redistribution of the electron density around Ga atoms.

Keywords: ZnO, radiofrequency magnetron sputtering, DFT, morphology, transparency, thin films.

1. Introduction

The interest in materials based on zinc oxide (ZnO) is related to its unique properties: a wide direct bandgap [1, 2], high transparency in the visible range [3, 4], high electrical conductivity [3], significant exciton binding energy (60 meV) [5, 6], *etc.* All of this leads to a wide range of ZnO applications: as hydrogen sensors [7], transparent conductive electrodes [8], piezoelectric sensors [9], *etc.*

A significant number of scientific publications focus on the investigation of ZnO thin films that can be used as an electron transport layer (ETL) in various photovoltaic and optoelectronic devices [10, 11]. Moreover, ZnO thin films have attracted considerable attention due to a number of important advantages in comparison to indium tin oxide (ITO)

Citation: Shulyma S.I., Sukhenko I.V., Kasyanenko V.Kh., Karbivskyy V.L., Kurgan N.A., Shvachko N.K., Zaika V.V., Moskaliuk V.O., Puzko O.A. Power-dependent evolution of structure and optical properties in gallium-doped ZnO magnetron sputtering thin films: experimental and DFT + U exploration. *Ukr. J. Phys.* **70**, No. 9, 609 (2025). https://doi.org/10.15407/ujpe70.9.609.

Fig. 1. Photo of GZO target for RF-magnetron sputtering

thin films: environmental safety [12, 13], low cost [12, 13], and the ability to be deposited on flexible substrates [14, 15].

However, unmodified ZnO films have certain disadvantages compared to ITO films, in particular: lower electrical conductivity [16], lower optical transparency (the average optical transparency of unmodified ZnO thin films is typically above 80% in the visible region [17, 18] in comparison with above 90% for ITO [19–21]), *etc.* Thus, there is a need to improve these ZnO thin films' properties for their potential applications.

To improve the optical and electrophysical properties of ZnO thin films, considerable attention is paid to their modification: doping [22–24], nanostructuring [25, 26], *etc.* One of the most accessible methods for enhancing the ZnO films properties is their doping with various elements: aluminum [27, 28], gallium [29, 30], indium [30], *etc.*

One of the most promising elements for the ZnO thin films doping is gallium (Ga), since its ionic radius ($r_{\text{ion}} = 0.47$ Å) is well matched to zinc ionic radius ($r_{\text{ion}} = 0.60$ Å). This facilitates the reduction of electron scattering on impurity atoms [16]. Furthermore, the incorporation of Ga into the ZnO lattice enhances the conductive properties of the films because Ga has three valence electrons (while Zn has two valence electrons).

There are various methods for producing ZnO thin films: chemical vapor deposition (CVD) [31], sol-gel method [32, 33], spray pyrolysis [34], *etc.* However, radiofrequency (RF) magnetron sputtering [14, 16, 27, 28] remains a relatively simple, easily scalable, and cost-effective method for the ZnO thin films formation, which allows to obtain highly uniform thin films. The magnetron power density during RF magnetron sputtering of thin films effects on their uniformity and density, and can also change their electrical and optical properties [35–37]. The formation peculiarities of undoped and doped ZnO thin films at different magnetron sputtering powers attract considerable interest to researchers because of the possibility of improving their characteristics, which will allow them to be used as ETL layers [35, 37, 38]. However, the available data on the formation peculiarities of such films remain insufficiently investigated and require further exploration and clarification.

This paper presents the experimental results of investigating the magnetron sputtering power density effect on the morphological and optical properties of gallium-doped ZnO (GZO) thin films obtained by RF magnetron deposition. Such studies are necessary to establish the optimal parameters (sputtering power density, optical and morphological properties *etc.*) for the formation of GZO thin films with improved properties.

To compare the experimental and theoretical results, quantum mechanical calculations were performed within the framework of density functional theory (DFT). Such calculations allowed us to explain some experimental results and verify the proposed hypotheses regarding the peculiarities of the GZO thin films formation at different magnetron sputtering powers. Furthermore, the DFT method made it possible to study the change in ZnO band structure and its density of states at doping with different gallium concentrations.

2. Methods of Synthesis and Characterization

The GZO thin films' deposition was carried out by bottom-up RF magnetron sputtering method. ZnO powder (99.9% purity) was mixed with dispersed Ga particles (99.9% purity) in a weight ratio 97 : 3, respectively. The average size of the dispersed Ga particles was ∼100–200 μm. The resulting mixture was pressed into a disk with a diameter 4.0 cm (Fig. 1) using a hydraulic press with a pressure of 796 kg/cm^2 to form the target, which was transported to the vacuum universal post (VUP-5M) chamber for synthesis. Since metallic Ga is ductile and fusible (Ga melting point is ∼29.8°C) even at room temperature, large Ga agglomerates (average size ∼1–2 mm) were observed in the obtained targets after pressing.

Slide glasses (1×1 cm^2, Rollmed, China) were used as substrates for the thin films, which were previously cleaned with acetone and isopropyl alcohol in an ultrasonic bath for 20 minutes and then rinsed with deionized water. After that, the substrates were transported to a vacuum chamber and placed above the target at a distance 4.5 ± 0.1 cm. A high vacuum (5.0×10^{-5} Pa) in the VUP-5M chamber was created by a rotary vane vacuum pump and diffusion pump with a cryogenic nitrogen trap. Argon (99.9% purity) was used to produce the plasma. The pressure inside the chamber during deposition was 1.0 Pa. GZO thin films were deposited at different magnetron power densities: $S = 9.55$ W/cm^2 (magnetron power $P =$ $= 120$ W), $S = 11.9$ W/cm^2 ($P = 150$ W), and $S = 15.9$ W/cm^2 ($P = 200$ W). In order to obtain thin films with a given thickness (∼500 nm), the deposition time (t) at different magnetron power densities was different: for $S = 9.55$ W/cm^2 – $t = 60$ minutes, for $S = 11.9$ W/cm^2 – $t = 30$ minutes, and for $S = 15.9$ W/cm^2 – $t = 30$ minutes.

The morphological analysis of GZO thin films surfaces was performed by scanning electron microscopy (SEM) using a Tescan Mira 3 microscope with an accelerating voltage of 5 to 20 kV. For SEM cross-sectional images obtaining, the films were destroyed by scratching the film surface with a scalpel and transported to carbon tape, where the images were acquired. Energy dispersive X-ray (EDX) studies were performed using an built-in Oxford X-max 80 mm^2 setup.

Spectrophotometric studies of the samples were performed on a single-beam UV-vis-NIR spectrophotometer Spekol 1500 in the wavelength range 190–1100 nm (scanning step 1 nm). The slide glass was used as the measurement reference for the optical transmittance.

Quantum mechanical calculations were performed using the Quantum ESPRESSO package [39–41]. GGA-PBEsol [42] was used as an exchange-correlation pseudopotential. In order to better describe localized states and prevent excessive hybridization, the DFT + U approach [43] applied Hubbard corrections to the 3*d* zinc, 2*p* oxygen, and 3*d* gallium states, which were 9.5 eV, 7.5 eV, and 7.0 eV, respectively. It was shown in [44, 45] that these values best reproduce the experimental results. The following model crystals were considered: ZnO, GZO (1 at.%) (Ga dopant concentration – 1 at.%), GZO (2.8 at.%) (Ga dopant concentration – 2.8 at.%). To simulate the doped crystals, ZnO supercells were constructed: $5 \times 5 \times 1$ and $3 \times 3 \times 1$ for dopant concentrations of 1% and 2.8%, respectively; after that one of the zinc atoms was replaced by a dopant atom. The k-point density of the Brillouin zone was chosen as follows (sequentially for structural relaxation, self-consistent electronic density calculation, and density of states calculation): $8 \times 8 \times 6$, $8 \times 8 \times 6$, $16 \times 16 \times 12$ for ZnO; $1 \times 1 \times 3$, $3 \times 3 \times 9$, $5 \times 5 \times 15$ for GZO(1 at.%); $1 \times 1 \times 2$, $3 \times 3 \times 6$, and $5 \times 5 \times 10$ for GZO(2.8 at.%). The plane-wave cutoff energy parameter was 1224 eV for undoped ZnO and 952 eV for supercells.

3. Results and Discussion

Figure 2 shows SEM images of the GZO thin films' surfaces obtained at different magnetron power values: $P = 120$ W: 120W-GZO sample (Fig. 2, *a*), $P = 150$ W: 150W-GZO sample (Fig. 2, *b*), and $P =$ $= 200$ W: 200W-GZO sample (Fig. 2, *c*). The characteristic surface morphology of the obtained thin films is a developed surface consisting of densely packed clusters of different sizes. The average size ($\bar{l}$) decreased with increasing magnetron sputtering power density.

The clusters' shape varies from almost round to elongated ellipse (Fig. 2, *a*–*c*). All films are characterized by the absence of foreign inclusions. An increasing magnetron sputtering power density leads to decrease in the clusters' size on the film surface. The clusters' average longitudinal sizes ($\bar{l}_1$) (along the y-axis in Fig. 2) for 120W-GZO, 150W-GZO, and 200W-GZO thin films are $(\bar{l}_1) = 91.1 \pm 23.4$ nm, $(\bar{l}_1) = 55.0 \pm 15.0$ nm and $(\bar{l}_1) = 46.8 \pm 11.9$ nm, respectively; and the average transverse sizes ($\bar{l}_2$) (along the x-axis in Fig. 2) are $(\bar{l}_2) = 65.2 \pm 8.9$ nm, $(\bar{l}_2) = 34.3 \pm 6.4$ nm, and $(\bar{l}_2) = 30.5 \pm 9.6$ nm, respectively.

Columnar growth is characteristic for all the studied thin films (Fig. 3). It confirms the texture of 120W-GZO, 150W-GZO and 200W-GZO thin films. As demonstrated in [46–48], ZnO films grow by the Volmer—Weber mechanism during magnetron sputtering. The columnar crystallite structure orientation corresponds to the [002] direction for both doped and undoped ZnO thin films [2, 46–48]. The formation of a columnar crystallite structure perpendicular to the substrate surface (Fig. 3, *a*–*c*), which

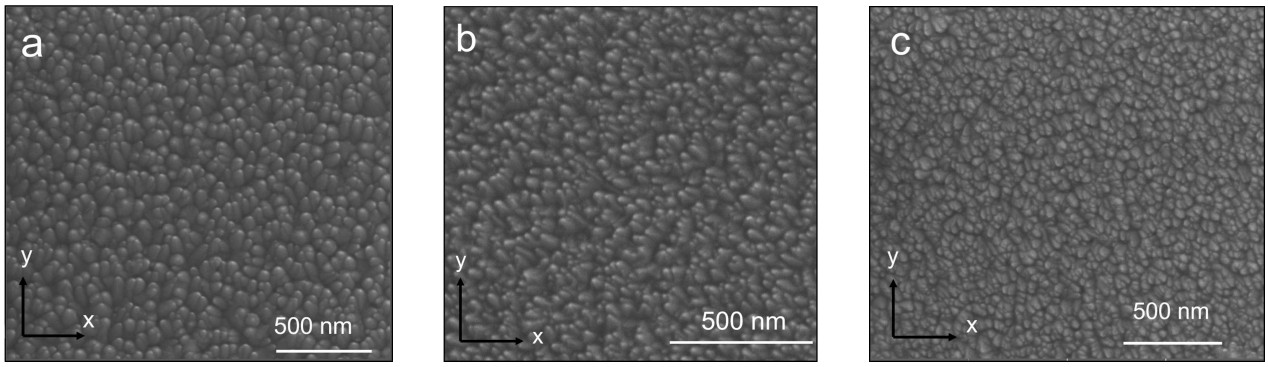

Fig. 2. SEM surface images of thin films: 120W-GZO (a), 150W-GZO (b), 200W-GZO (c)

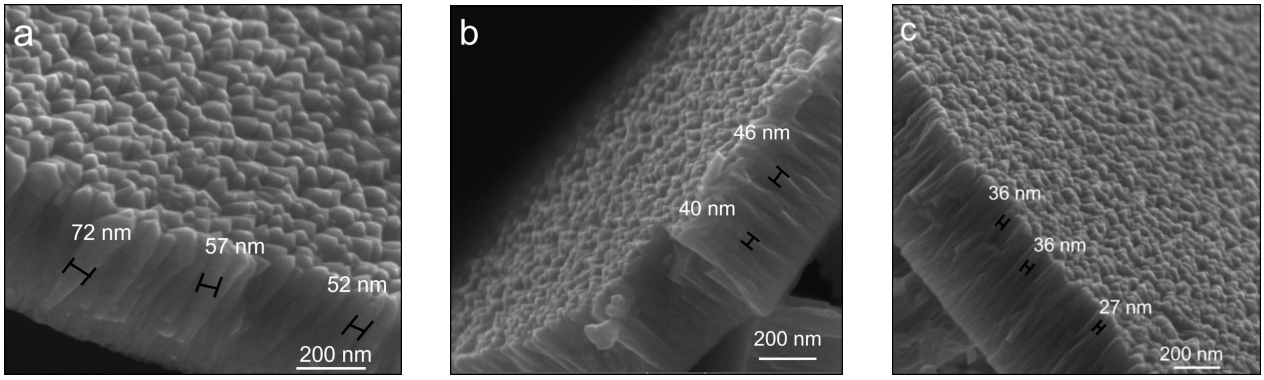

Fig. 3. SEM cross-sectional images of thin films: 120W-GZO (a), 150W-GZO (b), 200W-GZO (c). The structured grain-like formations are shown on the film's top surface

aligns with the [002] direction of ZnO, supports the occurrence of this growth mode.

An increase in the magnetron power density during the thin films deposition leads to a decrease in the average column thickness ($\bar{d}$) (Fig. 3): for 120W-GZO ($\bar{d}$) $= 62.2 \pm 16.6$ nm, for 150W-GZO ($\bar{d}$) $= 40.8 \pm$ $\pm\, 4.5$ nm, and for 200W-GZO – ($\bar{d}$) $= 29.2 \pm 5.9$ nm. At the final stages of growth, the columns end in either round or elongated elliptical clusters on the film surface. The clusters' size and shape depend on the sputtering power density (as shown above). Thus, higher power promotes the formation of smaller and denser clusters due to the increased number of atoms sputtered from the target.

The thicknesses of 120W-GZO, 150W-GZO, and 200W-GZO thin films were determined from SEM images of their cross-section (Fig. 4) and were equal to 486 nm, 425 nm, and 497 nm, respectively. Taking into account the film deposition time, the thin film growth rate R was calculated as a function of the magnetron power. The growth rate R for 120-GZO, 150W-GZO, and 200W-GZO thin films was $R =$ 8.1 nm/min, $R = 14.2$ nm/min, and $R = =$ 16.5 nm/min, respectively.

Thus, by changing the magnetron sputtering power density and measuring the deposition time, it is possible to form films with predetermined structural parameters: film thickness, crystallites' columnar structure width, and surface clusters' size.

To determine the chemical composition of the thin films, a quantitative chemical analysis by EDX was performed (Table 1). The results were compared with EDX data for undoped ZnO thin films obtained by RF magnetron sputtering at a magnetron power density $S = 9.55$ W/cm^2 ($P = 120$ W): 120W-ZnO samples (Table 1).

An oxygen deficiency was observed in the bulk of 120W-ZnO and 120W-GZO thin films. Such oxygen deficiency can be explained by both the presence of oxygen vacancies and interstitial zinc atoms. The

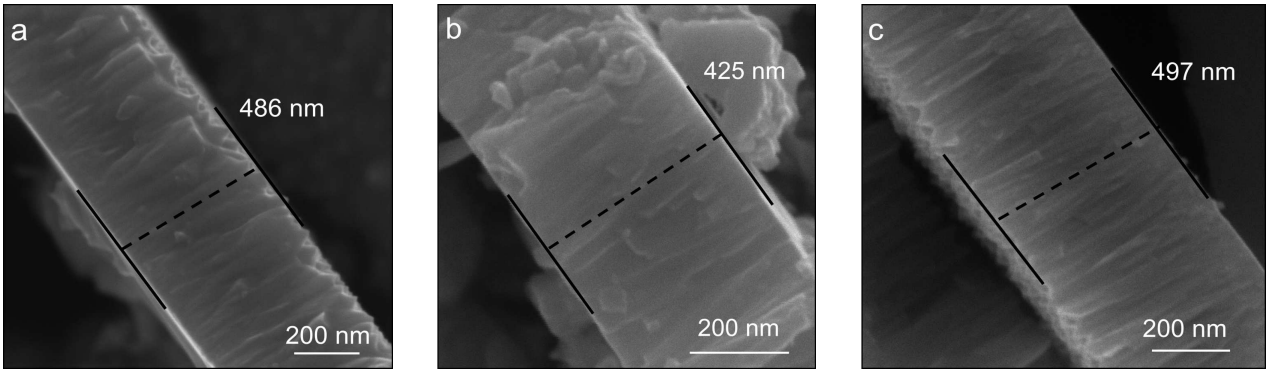

Fig. 4. SEM images of thin films and thickness measurements: 120W-GZO (*a*), 150W-GZO (*b*), 200W-GZO (*c*)

Ga doping at the same magnetron power density ($S = 9.55$ W/cm^2) did not lead to a significant change in the oxygen concentration (c_{O}) and was within the measurement error (Table 1). In contrast to oxygen, a decrease in the Zn concentration (c_{Zn}) with a simultaneous Ga concentration increase (c_{Ga}) was observed for 120W-GZO thin films compared to undoped ZnO films. This behavior confirms the replacement of Zn ions by Ga ions in the crystal lattice during the formation of doped GZO thin films.

A significant oxygen concentration increase was observed along with a sharp decrease in zinc concentration for 150W-GZO compared to 120W-GZO thin films. Moreover, at magnetron power densities $S = 11.9$ W/cm^2 and $S = 15.9$ W/cm^2 an increase in the Ga concentration was observed for 150W-GZO and 200W-GZO thin films (Table 1) that were equal to $c_{\mathrm{Ga}} = 1.08 \pm 0.05$ at.% and $c_{\mathrm{Ga}} = 1.5 \pm 0.01$ at.%, respectively. To explain this behavior, a model of thin film formation with increasing magnetron power density was proposed.

It is known that the magnetron power density increasing leads to an increase in temperature and plasma density. Since the dependence of the plasma thermal power on the magnetron deposition power density is linear [49], an increase in the magnetron deposition power should result in an increase in the target temperature. Moreover, such an enhancement leads to an increase in the substrate temperature. Purposeful target heating during sputtering was not performed, but it is known that a plasma temperature increase (and thus the target temperature) leads to a raising the temperature of deposited films during film synthesis [50]. That's why the temperature of the substrate during magnetron deposition was determined solely by the energy of plasma ions reaching the samples' surface. Furthermore, there is an enhancement in the number of high-energy argon ions, which transfer more energy to the target (ZnO/Ga) during the collision. The influence of these factors leads to the effect that at $S = 11.9$ W/cm^2, partial dissociation of ZnO in the gas phase (average Zn–O bond dissociation energy is roughly 280–290 kJ/mol [51]) can occur, while at a lower power ($S = 9.55$ W/cm^2 and below), the energy of argon ions is sufficient only to knock out ZnO molecules from the powder target. As a result, during the formation of thin films under intense plasma excitation ($S = 11.9$ W/cm^2 and above), the stoichiometry in the ratio between zinc and oxygen is disturbed. Thus, this leads to the appearance of excess oxygen in the deposited films, which is incorporated in the ZnO crystal lattice interstitial sites. Such an oxygen excess was observed for 150W-GZO thin films (Table 1).

Besides, the average Ga–O bond dissociation energy is 354–376 kJ/mol and it is slightly higher than Zn–O bond dissociation energy [51]. That means that gallium oxide formation in Ga–Zn–O plasma is slightly preferable than Zn–O. However, given the rel-

Table 1. **Elemental analysis data of thin films**

Sample	Element		
	O (at.%)	Zn (at.%)	Ga (at.%)
120W-ZnO	45.37 ± 0.87	54.73 ± 0.87	–
120W-GZO	47.84 ± 1.56	51.32 ± 1.58	0.84 ± 0.02
150W-GZO	62.62 ± 3.27	36.3 ± 2.97	1.08 ± 0.05
200W-GZO	57.07 ± 0.58	41.43 ± 0.59	1.50 ± 0.01

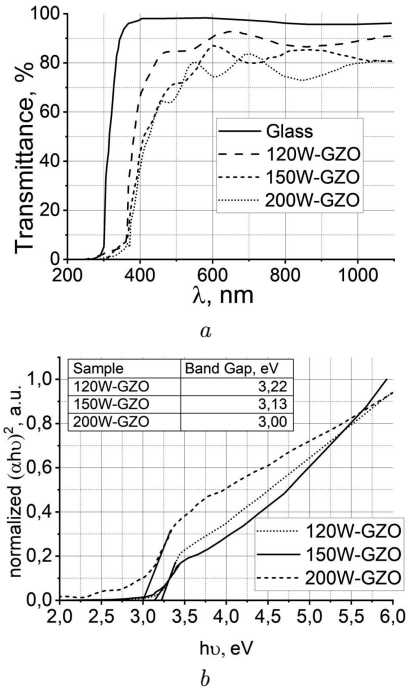

Fig. 5. GZO thin films optical transmission spectra (a), an optical band gap determination by the Tauc method (b). λ is the optical radiation wavelength

atively small concentration of Ga in the initial target, the probability of such formation is negligible.

A slight increase in zinc concentration with a simultaneous decrease in oxygen concentration was observed for 200W-GZO compared to 150W-GZO thin films (Table 1). Such behavior, in our opinion, is due to the partial recombination of oxygen into O_2, which is more difficult to attach to the substrate. Since the typical O_2 bond formation energy (∼498–499 kJ/mol [51]) is bigger than for Zn-O and Ga-O bonds dissociation energies and taking into consideration a significant quantity of oxygen in initial target (almost 50%) than O_2 formation at such conditions are quite probable. Moreover, there may be an interstitial zinc concentration enhancement with an increase in the power of magnetron sputtering. Since Zn ions can be placed in the ZnO crystal lattice interstitial sites under its heating [52], the magnetron power density increase to $S = 15.9$ W/cm^2 leads to the appearance of a larger number of interstitial Zn ions during GZO thin films formation. Thus, all this, in our opinion, leads to the c_{Zn} increase in 200W-GZO compared to 150W-GZO thin films.

Since the ZnO/Ga target formation process involved intensive mixing of the mixture components, heavier Ga particles settled down in the deeper mixtures layers. Therefore, the Ga agglomerates concentration in the pressed targets was also higher in the deeper target layers. The magnetron power density enhancement causes the ZnO/Ga target sputtering with higher-energy argon ions and this process accompanied by the plasma temperature increasing. Therefore, the low-melting Ga was able to evaporate more intensively and from deeper target layers with higher Ga agglomerates concentration.

To determine the RF magnetron sputtering power effect on the optical properties of the investigated films, optical transmission spectra were obtained (Fig. 5, a). The optical bandgap width E_g investigated thin films were determined by using the Tauc method [53, 54] (Fig. 5, b). The E_g value can be calculated by the equation [27, 55, 56]:

$$(\alpha h\nu)^{1/\gamma} = B(h\nu - E_g), \tag{1}$$

where α is the absorption coefficient, ν is the optical radiation frequency, h is Planck's constant, B is the characteristic constant, and γ is a parameter related to the type of electronic transition. Since ZnO is a semiconductor with a direct bandgap, $\gamma = 1/2$ [56].

All the analyzed thin films are characterized by high transparency in the visible and near-infrared ranges (Fig. 5, a). The maximum value of optical transparency was observed for 120W-GZO films and was equal to $92.8 \pm 0.5\%$. GZO thin films deposited at higher magnetron power density manifested lower optical transparency values. Such behavior for higher S values is associated with the crystallites' grain size decreasing on the surface and in the volume of thin films (Figs. 2, 3) and following the light scattering increasing at the such grain boundaries.

A slight increase of E_g to 3.22 ± 0.01 eV was observed for 120W-GZO thin films (inset Fig. 5, b) compared to undoped 120W-ZnO films with optical band gap $E_g = 3.20 \pm 0.01$ eV [46]. Since, as shown above, the replacement of Zn ions in the ZnO lattice during the 120W-GZO thin films magnetron sputtering occurs primarily with Ga ions, such an increase in E_g can be explained by the population of unoccupied states at the bottom of the ZnO conduction band with free electrons from Ga (the Moss–Berstein effect [57, 58]).

The magnetron sputtering power increase leads to the decreasing of E_g value (Fig. 5, *b*). The optical band gap value was $E_g = 3.13 \pm 0.01$ eV and $E_g = 3.00 \pm 0.0$ eV for 150W-GZO samples and 200W-GZO samples, respectively.

As noted above, 150W-GZO thin films are characterized by an excess of oxygen compared to 120W-GZO thin films (Table 1), which, in our opinion, is partially placed in the crystal lattice interstitial positions. This leads to the appearance of acceptor impurity levels [59], which form localized electronic states in the band gap near the valence zone. The appearance of such impurity levels causes the optical band gap value to decrease.

The fact that the magnetron power density enhancement to $P = 200$ W (200W-GZO thin films) causes a further decrease in the value of E_g (Fig. 5, *b*) is associated with the growing amount of interstitial zinc in the ZnO crystal lattice. Such defects act as donor impurities, creating additional electronic states near the bottom of the conduction band [60]. As a result, the optical band gap value E_g decreases to 3.00 ± 0.01 eV.

To verify the proposed hypotheses regarding GZO thin films formation peculiarities at different magnetron powers, as well as the influence of internal structure changes on their optical and structural properties the calculation using the DFT + U theory was performed. As shown from the EDX results (Table 1), the magnetron sputtering power density enhancement leads to Ga concentration increasing for investigated GZO thin films under the given experimental conditions. Since ZnO thin films doping with Ga results in Zn^{2+} replacement by Ga^{3+} in the crystal lattice, the initial model crystal was selected and calculated based on these considerations (Fig. 6, *a* – calculation of the model crystal for GZO(1 at.%) within the DFT + U theory framework). The total and partial density of states (DOS) for undoped ZnO and doped with different gallium concentrations ZnO (GZO (1 at.%) and GZO (2.8 at.%)) thin films have been investigated within the framework of the DFT + U theory (Fig. 6, *b*).

The valence band upper part almost entirely consisted of 2*p* oxygen states, but the valence band middle part consisted of 3*d* zinc states (Fig. 6, *b*) for both undoped and gallium-doped ZnO crystal lattices. However, gallium doping of ZnO led to the appearance of additional electronic states in the vicinity of –5.0 eV

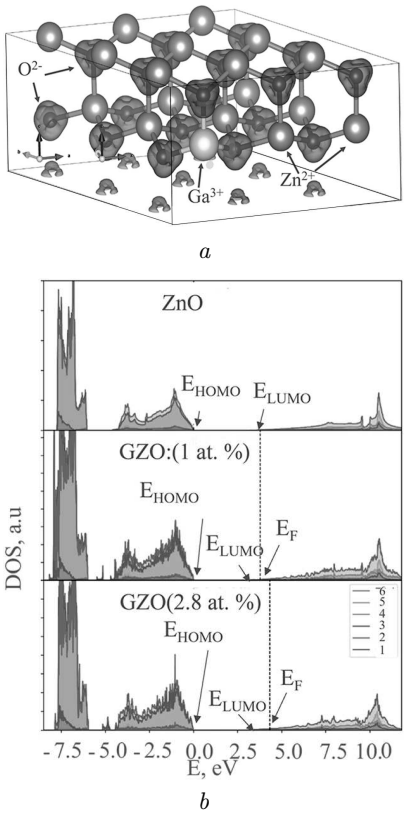

Fig. 6. An example of a model crystal GZO(1 at.%) for DOS calculations within the framework of the DFT + U theory (*a*). Valence and conduction bands total and partial densities of states for ZnO, GZO (1 at.%), GZO (2.8 at.%) compounds (*b*): O 2*p* states (*1*), O 2*s* states (*2*), Zn 3*d* states (*3*), Zn 4*p* states (*4*), Zn 4*s* states (*5*), total density of states (*6*). E_{HOMO} is the highest occupied molecular orbital energy, E_{LUMO} is the lowest unoccupied molecular orbital energy, E_{F} is the Fermi energy (the dotted line shows the Fermi level position)

in the valence band, which were formed by Zn 3*d* and O 2*p* states. Such appearance of additional electronic states can be attributed to the following physical mechanisms: 1) 3*d* Zn and 2*p* O states hybridization with 4*s* and 4*p* Ga states, which leads to new energy levels formation; 2) 3*d* Zn and 2*p* O energy levels position shift due to changes in interatomic distances and bond symmetry (Fig. 6, *a*); 3) the electron density redistribution around impurity atoms, since Ga has a different electronic configuration ($3d^{10}4s^24p^1$) compared to Zn ($3d^{10}4s^2$), which can affect the electronic structure of the crystal lattice.

The ZnO, GZO (1 at.%) and GZO (2.8 at.%) conduction bands almost entirely consisted of hybridized

Zn 4s, Zn 4p, and O 2p states (Fig. 6, b). The slight decrease in energy gap $\Delta(E_{\mathrm{LUMO}} - E_{\mathrm{HOMO}})$ with Ga dopant concentration enhancement was observed (Fig. 6, b, Table 2).

Ga is characterized by the presence of Ga 4s and Ga 4p states whose interaction with ZnO electronic states can cause hybridization of electronic states. It can lead to a decrease in the energy gap ($\Delta(E_{\mathrm{LUMO}} - E_{\mathrm{HOMO}})$). Moreover, Ga doping causes a slight crystal lattice deformation and the local states' formation in the band gap, which can lead to the band structure changes (Fig. 6, b).

At the same time, the Fermi level shifts to the conduction band (Fig. 6, b, Table 2) for GZO samples. The Ga concentration enhancement in the GZO crystal structure caused a significant increase in the energy distance $\Delta(E_{\mathrm{F}} - E_{\mathrm{HOMO}})$ between the Fermi level (E_{F}) and the highest occupied molecular orbital level (E_{HOMO}). Such behavior is due to Ga electrons occupying the free states in the lower part of the ZnO conduction band. Since gallium has three valence electrons but zinc has only two, gallium doping of ZnO increases free electrons concentration in the material. Such $\Delta(E_{\mathrm{F}} - E_{\mathrm{HOMO}})$ increasing is manifested in the optical band gap E_g magnification with Ga dopant concentration increasing (Moss–Berstein effect [57, 58]), which was experimentally observed for 120W-GZO samples compared to undoped ZnO thin films.

The experimental and DFT + U simulation results show opposite trends concern the Ga dopant concentration effect on the optical bandgap value E_g. In the experiment, the magnetron sputtering power enhancement caused the Ga concentration increasing and the optical band gap E_g decreasing (Fig. 5, b). Instead, in the DFT + U simulation, the Ga concentration increasing caused the optical band gap E_g magnification (Fig. 6, b, Table 2).

Thus, the Ga dopant concentration increasing cannot be the cause of E_g decreasing with an increase in the magnetron sputtering power. Such a decrease in the optical band gap can occur due to the interstitial defects appearing in the ZnO crystal lattice, which lead to the impurity levels formation in the band gap. However, the simulated structure in the DFT + U calculations was more idealized and the equilibrium configuration did not take into account the interstitial defects.

Table 2. **Theoretical energy gaps**

Sample	$\Delta E_{\mathrm{LUMO-HOMO}}$	$\Delta E_{\mathrm{F-HOMO}}$
ZnO	3.06	–
ZnO : Ga (1 at.%)	2.97	3.79
ZnO : Ga (2.8 at.%)	2.90	4.32

4. Conclusions

It is shown that Ga ions replace Zn ions in the ZnO crystal lattice during the gallium doping of ZnO thin films (for $S = 9.55$ W/cm^2). Magnetron sputtering power density enhancement to $S = 11.9$ W/cm^2 and $S = 15.9$ W/cm^2 lead to increase of Ga concentration to 1.08 ± 0.05 at.% and 1.50 ± 0.01 at.% in GZO thin films, respectively. It is found that the increase in sputtering power density leads to decreasing the size of clusters on the film surface and the thickness of the crystallites' columnar structure of Ga-doped ZnO thin films.

The GZO thin films' formation mechanism at different magnetron sputtering power density is proposed. The excess oxygen at a magnetron power density $S = 11.9$ W/cm^2 is placed in ZnO crystal lattice interstitial positions and forms acceptor levels in its band gap. The magnetron sputtering power density enhancement to $S = 15.9$ W/cm^2 causes an increase in the number of interstitial Zn ions (due to the sputtering temperature increase). It leads to the formation of additional defects in the ZnO crystal lattice.

It is established that the optical band gap E_g decreasing from 3.22 ± 0.01 eV (for $S = 9.55$ W/cm^2) to 3.00 ± 0.01 eV (for $S = 15.9$ W/cm^2) with increasing magnetron sputtering power density is due to the interstitial defects formation and the impurity levels appearance in the band gap.

Quantum mechanical DFT + U calculations have confirmed that an increase in the Ga concentration does not lead to a decrease in E_g, but, on the contrary, it can increase E_g due to the Moss–Berstein effect. Instead, the experimentally observed E_g decrease may be due to the interstitial defects formation in the ZnO crystal lattice, which were not taken into consideration during DFT + U simulation.

The authors acknowledge the financial support of the National Academy of Sciences of Ukraine, Project No. 3-A (0125U000325).

1. D. Banerjee, J.Y. Lao, D.Z. Wang, J.Y. Huang, Z.F. Ren, D. Steeves, B. Kimball, M. Sennett. Large-quantity free-standing ZnO nanowires. *Appl. Phys. Lett.* **83**, 2061 (2003).
2. K.M. Sandeep, S. Bhat, S.M. Dharmaprakash. Structural, optical, and LED characteristics of ZnO and Al doped ZnO thin films. *J. Phys. Chem. Solids* **104**, 36 (2017).
3. N. Mursal, N. Irhamni, N. Bukhari, Z. Jalil. Structural and optical properties of zinc oxide (ZnO) based thin films deposited by sol-gel spin coating method. *J. Phys. Conf. Ser.* **1116**, 032020 (2018).
4. C. Agashe, O. Kluth, G. Schöpe, H. Siekmann, J. Hüpkes, B. Rech. Optimization of the electrical properties of magnetron sputtered aluminum-doped zinc oxide films for opto-electronic applications. *Thin Solid Films* **442**, 167 (2003).
5. M. Dvorak, S.-H. Wei, Z. Wu. Origin of the variation of exciton binding energy in semiconductors. *Phys. Rev. Lett.* **110**, 016402 (2013).
6. D.G. Thomas. The exciton spectrum of zinc oxide. *J. Phys. Chem. Solids* **15**, 86 (1960).
7. P. Mitra, A.P. Chatterjee, H.S. Maiti. ZnO thin film sensor. *Mater. Lett.* **35**, 33 (1998).
8. A. Tubtimtae, M.-W. Lee. ZnO nanorods on undoped and indium-doped ZnO thin films as a TCO layer on nonconductive glass for dye-sensitized solar cells. *Superlattices Microst.* **52**, 987 (2012).
9. V. Polewczyk, R.M. Maffei, G. Vinai, M. Cicero, S. Prato, P. Capaldo, S.D. Zilio, A. Bona, G. Paolicelli, A. Mescola, S. D'Addato, P. Torelli, S. Benedetti. ZnO thin films growth optimization for piezoelectric application. *Sensors* **21**, 6114 (2021).
10. C. Qiu, Y. Wu, J. Song, W. Wang, Z. Li. Efficient planar perovskite solar cells with zno electron transport layer. *Coatings* **12**, 1981 (2022).
11. D.C. Tiwari, S.K. Dwivedi, P. Dipak, T. Chandel, R. Sharma. Sol-gel derived ZnO as an electron transport layer (ETL) for inverted organic solar cells. In: *AIP Conference Proceedings, Provo, Utah, USA, July 16–21, 2017*, p. 060024-1.
12. Ü. Özgür, Ya. I. Alivov, C. Liu, A. Teke, M.A. Reshchikov, S. Doğan, V. Avrutin, S.-j. Cho, H. Morkoç. A comprehensive review of ZnO materials and devices. *J. Appl. Phys.* **98**, 041301 (2005).
13. A. Kolodziejczak-Radzimska T. Jesionowski. Zinc Oxide-From Synthesis to Application: A review. *Materials* **7**, 2833 (2014).
14. Y.J. Kim, H.S. Lee, J.-S. Noh. Transient behaviors of ZnO thin films on a transparent, flexible polyethylene terephthalate substrate. *Thin Solid Films* **603**, 160 (2016).
15. P.-H. Lei, H.-M. Wu, C.-M. Hsu. Zinc oxide (ZnO) grown on flexible substrate using dual-plasma-enhanced metalorganic vapor deposition (DPEMOCVD). *Surf. Coat. Tech.* **206**, 3258 (2012).
16. K. Ellmer, R. Mientus. Carrier transport in polycrystalline transparent conductive oxides: A comparative study of zinc oxide and indium oxide. *Thin Solid Films.* **516**, 4620 (2008).
17. L.C. Nehru, M. Umadevi, C. Sanjeeviraja. Studies on structural, optical and electrical properties of ZnO thin films prepared by the spray pyrolysis method. *Int. J. Mater. Eng.* **2**, 12 (2012).
18. N. Mursal, N. Irhamni, N. Bukhari, Z. Jalil. Structural and optical properties of zinc oxide (ZnO) based thin films deposited by sol-gel spin coating method. *J. Phys.: Conf. Ser.* **1116**, 032020 (2018).
19. T.M. Hammad. Effect of annealing on electrical, structural, and optical properties of sol–gel ITO thin films. *Phys. Status Solidi (A) Appl. Mater. Sci.* **206**, 2128 (2009).
20. C. Guillen, J. Herrero. Comparison study of ITO thin films deposited by sputtering at room temperature onto polymer and glass substrates. *Thin Solid Films* **480–481**, 129 (2004).
21. J.H. Kim, K.A. Jeon, G.H. Kim, S.Y. Lee. Electrical, structural, and optical properties of ITO thin films prepared at room temperature by pulsed laser deposition. *Appl. Surf. Sci.* **252**, 4834 (2005).
22. X. Liu *et al.* In-doped ZnO electron transport layer for High-Efficiency ultrathin flexible organic solar cells. *Adv. Sci.* **11**, 2402158 (2024).
23. A.K. Ambedkar, M. Singh, V. Kumar, V. Kumar, B.P. Singh, A. Kumar, Y.K. Gautam. Structural, optical and thermoelectric properties of Al-doped ZnO thin films prepared by spray pyrolysis. *Surf. Interfaces.* **19**, 100504 (2020).
24. S.D. Ponja, S. Sathasivam, I.P. Parkin, C.J. Carmalt. Highly conductive and transparent gallium doped zinc oxide thin films via chemical vapor deposition. *Sci. Rep.* **10**, 638 (2020).
25. G. Bagha, K. Samavati, H. Naffakh-Moosavy, L.F. Matin. Controlling surface morphology of Ag-doped ZnO as a buffer layer by dispersion engineering in planar perovskite solar cells. *Sci. Rep.* **14**, 4617 (2024).
26. W.B. Tarique, M.H. Rahaman, S.S. Dipta, A.H. Howlader, A. Uddin. Solution-Processed bilayered ZnO electron transport layer for efficient inverted Non-Fullerene organic solar cells. *Nanomanufacturing* **4**, 81 (2024).
27. V.V. Zaika, N.K.Shvachko, V.H. Kasiyanenko, V.L. Karbivskyy, V.O. Moskaliuk, I.V. Sukhenko, A.P. Soroka. The influence of aluminum on the morphological, optical properties and electronic structure of ZnO thin films. *Funct. Mater.* **31**, 185 (2024).
28. A.I. Kashuba, B. Andriyevsky, H.A. Ilchuk, R.Yu. Petrus, T.S. Malyi, I.V. Semkiv. Optical and dispersion parameters of the al-doped ZnO thin film. *J. Nano-Electron. Phys.* **13**, 04006 (2021).
29. P. Nunes, E. Fortunato, P. Tonello, F.B. Fernandes, P. Vilarinho, R. Martins. Effect of different dopant elements on the properties of ZnO thin films. *Vacuum* **64**, 281 (2002).

30. D.K. Kim. Characteristics of Ga doped ZnO thin films deposited by RF magnetron sputtering with base pressure. *Appl. Sci. Converg. Technl.* **28**, 13 (2019).
31. J. Hu, R.G. Gordon. Textured aluminum-doped zinc oxide thin films from atmospheric pressure chemical-vapor deposition. *J. Appl. Phys.* **71**, 880 (1992).
32. J.N. Hasnidawani, H.N. Azlina, H. Norita, N.N. Bonnia, S. Ratim, E.S. Ali. Synthesis of ZnO nanostructures using Sol-Gel method. *Procedia Chem.* **19**, 211 (2016).
33. S.A. Kamaruddin, K.-Y. Chan, H.-K. Yow, M.Z. Sahdan, H. Saim, D. Knipp. Zinc oxide films prepared by sol-gel spin coating technique.*Appl. Phys. A* **104**, 263 (2010).
34. M. Krunks, E. Mellikov. Zinc oxide thin films by the spray pyrolysis method. *Thin Solid Films* **270**, 33 (1995).
35. R.S. Gonçalves, P. Barrozo, F. Cunha. Optical and structural properties of ZnO thin films grown by magnetron sputtering: Effect of the radio frequency power. *Thin Solid Films* **616**, 265 (2016).
36. M.K. Khalaf, H.F. Al-Taay, D.S. Ali. Effect of radio frequency magnetron sputtering power on structural and optical properties of Ti6Al4V thin films. *Photonic Sens.* **7**, 163 (2017).
37. N. Srinatha, Y.S. No, V.B. Kamble, S. Chakravarty, N. Suriyamurthy, B. Angadi, A.M. Umarji, W.K. Choi. Effect of RF power on the structural, optical and gas sensing properties of RF-sputtered Al doped ZnO thin films. *RSC Adv.* **6**, 9779 (2016).
38. X. Yu, J. Ma, F. Ji, Y. Wang, X. Zhang, C. Cheng, H. Ma. Effects of sputtering power on the properties of ZnO : Ga films deposited by r.f. magnetron-sputtering at low temperature. *J. Crys. Growth* **274**, 474 (2004).
39. P. Giannozzi *et al.* QUANTUM ESPRESSO: A modular and open-source software project for quantum simulations of materials. *J. Condens. Matter Phys.* **21**, 395502 (2009).
40. P. Giannozzi *et al.* Advanced capabilities for materials modelling with Quantum ESPRESSO. *J. Condens. Matter Phys.* **29**, 465901 (2017).
41. P. Giannozzi *et al.* Quantum ESPRESSO toward the exascale. *J. Chem. Phys.* **152**, 154105 (2020).
42. J.P. Perdew, A. Ruzsinszky, G.I. Csonka, O.A. Vydrov, G.E. Scuseria, L.A. Constantin, X. Zhou, K. Burke. Restoring the density-gradient expansion for exchange in solids and surfaces. *Phys. Rev. Lett.* **100**, 136406 (2008).
43. S.L. Dudarev, G.A. Botton, S.Y. Savrasov, C.J. Humphreys, A.P. Sutton. Electron-energy-loss spectra and the structural stability of nickel oxide: An LSDA + U study. *Phys. Rev. B* **57**, 1505 (1998).
44. D.A. Leon, C. Elgvin, P.D. Nguyen, Ø. Prytz, F.S. Hage, K. Berland. Unraveling many-body effects in ZnO: Combined study using momentum-resolved electron energy-loss spectroscopy and first-principles calculations. *Phys. Rev. B* **109**, 115153 (2024).
45. L. Dong, R. Jia, B. Xin, B. Peng, Y. Zhang. Effects of oxygen vacancies on the structural and optical properties of β-Ga_2O_3. *Sci. Rep.* **7**, 40160 (2017).
46. W. Gao, Z. Li. ZnO thin films produced by magnetron sputtering. *Ceram. Int.* **30**, 1155 (2004).
47. M. Nie, A. Bikowski, K. Ellmer. Microstructure evolution of Al-doped zinc oxide and Sn-doped indium oxide deposited by radio-frequency magnetron sputtering: A comparison. *J. Appl. Phys.* **117**, 155301 (2015).
48. Y. Sato, M. Taketomo, N. Ito, A. Miyamura, Y. Shigesato. Comparative study on early stages of film growth for transparent conductive oxide films deposited by dc magnetron sputtering. *Thin Solid Films* **516**, 4598 (2007).
49. K. Ellmer. Magnetron sputtering of transparent conductive zinc oxide: Relation between the sputtering parameters and the electronic properties. *J. Phys. D: Appl. Phys.* **33**, R17 (2000).
50. R. Graillot-Vuilecot, T. Anne-Lise, T. Lecas, C. Cachoncinlle, E. Millon, A. Caillard. Hot target magnetron sputtering process: Effect of infrared radiation on the deposition of titanium and titanium oxide thin films. *Vacuum* **181**, 109734 (2020).
51. *NIST-JANAF Thermochemical Tables* (4th ed.). Edited by M.W. Jr. Chase (American Institute of Physics, 1998) [ISBN: 978-156-3968-31-0].
52. F. Van Craeynest, W.M.D. Vorst, W. Dekeyser. Interpretation of the yellow colour of heat treated ZnO powder. *Phys. Status Solidi B* **8**, 841 (1965).
53. J. Tauc. Optical properties and electronic structure of amorphous Ge and Si. *Mater. Res. Bull.* **3**, 37 (1968).
54. J. Tauc, R. Grigorovici, A. Vancu. Optical properties and electronic structure of amorphous Germanium. Phys. *Status Solidi B* **15**, 627 (1966).
55. V. Karbivskyy, N. Kurgan, M. Hantusch, A. Romansky, I. Sukhenko, L. Karbivska. Design of the electronic structure and properties of calcium apatites via isomorphic modification of the cation sublattice, and prospects of their application. *J. Appl. Phys.* **135**, 065102 (2024).
56. G.G.N. Angilella, N.H. March, I.A. Howard, R. Pucci. Pressure dependence of the energy gaps in diamond-type semiconductors, and their III-V analogues such as InSb. *J. Phys. Conf. Ser.* **121**, 032006 (2008).
57. E. Burstein. Anomalous optical absorption limit in INSB. *Phys. Rev.* **93**, 632 (1954).
58. T.S. Moss. The interpretation of the properties of indium antimonide. *Proc. Phys. Soc. B* **67**, 775 (1954).
59. K.E. Knutsen, A. Galeckas, A. Zubiaga, F. Tuomisto, G.C. Farlow, B.G. Svensson, A.Yu. Kuznetsov. Zinc vacancy and oxygen interstitial in ZnO revealed by sequential annealing and electron irradiation. *Phys. Rev. B* **86**, 121203 (2012).
60. L. Schmidt-Mende, J.L. MacManus-Driscoll. ZnO – nanostructures, defects, and devices. *Mater. Today* **10**, 40 (2007).

Received 01.04.25

С.І. Шулима, І.В. Суханко, В.Х. Касьяненко, В.Л. Карбівський, Н.А. Курган, В.В. Заіка, В.О. Москалюк, О. А. Пузько

ЕВОЛЮЦІЯ СТРУКТУРИ ТА ОПТИЧНИХ ВЛАСТИВОСТЕЙ ТОНКИХ ПЛІВОК Ga-ЛЕГОВАНОГО ZnO, ОТРИМАНИХ МЕТОДОМ МАГНЕТРОННОГО НАПИЛЕННЯ З РІЗНОЮ ПОТУЖНІСТЮ: ЕКСПЕРИМЕНТ ТА МОДЕЛЮВАННЯ DFT + U

Досліджено вплив потужності радіочастотного магнетронного напилення на морфологію та оптичні властивості допованих галієм тонких плівок ZnO (GZO). Показано, що зі збільшенням потужності напилення зменшуються розміри кластерів на поверхні плівки та товщина стовпчастої структури кристалітів. Встановлено, що зменшення ширини оптичної забороненої зони може бути пов'язане з появою міжвузлових дефектів у кристалічній ґратці. Спостерігалося збільшення концентрації Ga в плівках GZO за сталого вагового співвідношення вихідних сумішей ZnO та Ga при зростанні потужності напилення. Запропоновано механізм формування тонких плівок GZO при збільшенні потужності магнетронного напилення, який пов'язаний з появою міжвузлових включень Zn і O в кристалічній ґратці ZnO. DFT-розрахунки (з поправкою Хаббарда, DFT + U) показали, що підвищена концентрація Ga не спричиняє звуження оптичної забороненої зони. Натомість, збільшення вмісту Ga приводить до появи додаткових електронних станів у валентній зоні (–5.0 еВ), що пов'язано з гібридизацією Zn 3*d* і O 2*p* з 4*s*- та 4*p*-станами Ga, зміною положення енергетичних рівнів Zn 3*d* та O 2*p* внаслідок зміни міжатомних відстаней та симетрії зв'язків і перерозподілом електронної густини навколо атомів Ga.

Ключові слова: ZnO, радіочастотне магнетронне напилення, DFT, морфологія, прозорість, тонкі плівки.